Preprints of the 21st IFAC World Congress (Virtual)
Berlin, Germany, July 12-17, 2020

Dynamic performance estimation: A design tool for mechatronic scanners

E. Csencsics and G. Schitter

Christian Doppler Laboratory for Precision Engineering for Automated In-line Metrology, Automation and Control Institute (ACIN), Vienna University of Technology, 1040 Vienna, Austria (e-mail: csencsics@acin.tuwien.ac.at).

Abstract:
This paper presents an integrated framework for the dynamic performance estimation (DPE) of mechatronic scanners in the design phase, which is based on frequency domain models of system components and signals in the system. It considers stochastic noise sources (e.g. sensor noise) as well as deterministic signals (e.g. reference trajectory) and propagates each signal to the desired performance output (e.g. actuator current) via obtained transfer functions. The framework is evaluated for a 2 inch fast steering mirror (FSM) dedicated as optical scanner by comparing estimated and measured values for positioning uncertainty, rms coil current and rms tracking error. The estimated positioning uncertainty for the FSM with a range of 52.4 mrad deviates only 0.74 μrad from the measured value. The estimated values for three tested raster trajectories also show good agreement with the measurements resulting in averaged relative deviations of 12% for the rms current values and between 15-17% for the rms tracking error.

Keywords: System analysis and design, Motion control, Fast steering mirrors

1. INTRODUCTION

In the design phase of mechatronic scanning systems a reliable estimation of the resulting performance of the feedback and/or feedforward controlled system is a valuable input for the designer. A reliable virtual prototyping framework enables (i) the cutting of costs in the design phase (ii) a speed-up of the design process and (iii) enhanced insights into the system design and the interrelations between components [Munnig Schmidt et al. (2014)]. Considerable research efforts have thus been invested into the development of generic computer-based design tools to predict the interaction between subsystems and consequences of design choices for mechatronic motion systems in the conceptual design phase [Coelingh et al. (1998)]. Approaches employing genetic algorithms for evaluating combinations of sub-concepts from mechanics and control [Avigad et al. (2003)] or a mechatronic design quotient as multicriteria index, reflecting the system-based evaluation of a mechatronic design, are reported [Behbahani and de Silva (2008)]. These more general design tools may provide good starting points for a system design but seem not applicable for shaping the properties of e.g. a particular high performance system.

Concepts more focused on predicting and optimizing the performance of mechatronic high precision systems include the prediction of the resolution in nano-positioning system from the measured closed-loop actuator voltage [Fleming (2014)] and the concept of dynamic error budgeting (DEB) for determining the resolution of high precision machines [Jabben (2007), Monkhorst (2004)]. The latter has been used frequently for analysis, design an optimization in several applications including PMSM driven telescope mounts [Riel et al. (2016)], one degree of freedom nano-metrology platforms [Saathof et al. (2017)] and long stroke linear nano-positioners [Okyay et al. (2018)], confining itself to stochastic disturbances. Both concepts target primarily the determination of the resulting steady state positioning uncertainty as the sole performance output of the system.

However, for mechatronic scanning systems, such as fast steering mirrors (FSMs) used in scanning optical sensors [Schlarp et al. (2019)] or material processing [Hedding and Lewis (1990)], there may be additional performance outputs, such as energy consumption or tracking error, which are of interest in the design phase. For systems tailored to a certain application e.g. the information on which trajectory type (raster, Lissajous, spiral, etc.) with which combinations of frequency and amplitude can be continuously tracked within the thermal limits of the actuator and power electronics may be of highest interest [Csencsics and Schitter (2017b)].

The contribution of this paper is an integrated framework enabling the dynamic performance estimation (DPE) of arbitrary performance outputs within a feedback and/or feed-forward controlled mechatronic system under the consideration of stochastic as well as deterministic signals. It is based on a frequency domain description of signals entering the system, allows the assessment of components and feasible scan trajectories and is experimentally validated using a commercial FSM.

2. DYNAMIC PERFORMANCE ESTIMATION

The DPE framework enables the prediction of arbitrary performance outputs of a mechatronic system based on

frequency domain models for components, i.e. transfer functions (TFs), and signals in the system, i.e. power spectral density (PSD) models. The DPE is able to consider deterministic signals in addition to stochastic signals and thus extends the idea of DEB [Jabben (2007)], determining the positioning uncertainty of a mechatronic system in standstill by considering only stochastic disturbances.

2.1 Stochastic signals (DEB)

In the DEB approach the single sided PSD is used to define the power of a signal per unit of frequency. For a time signal n(t) with zero mean the PSD $S_n(f)$ is linked to the variance (equaling the mean square value) by

$$\sigma_n^2 = x_{n,rms}^2 = \int_0^\infty S_n(f)df. \tag{1}$$

This relation resembles *Parseval's theorem* relating power in the time and frequency domain. The PSD of the signal n entering the system at a certain point can be propagated to a desired performance output y via

$$S_{n\to y}(f) = |G_{y,n}(j\omega)|^2 S_n(f) \tag{2}$$

with $G_{y,n}(s)$ being the transfer function from input n to output y. The resulting overall PSD at the performance output y can then be obtained by summation of the PSDs of all disturbances and signals in the system

$$S_y(f) = \sum_i |G_{y,n_i}(j\omega)|^2 S_{n_i}(f). \tag{3}$$

and the resulting rms value of the performance output can be calculated via (1).

2.2 Extension to deterministic signals (DPE)

When considering periodic signals the PSD will show infinite peaks (Dirac pulse), which hinders their consideration for a performance estimation in the frequency domain. In practice, however, these peaks will not be infinite, as the PSD of a periodic signal is calculated discretely, e.g. using the Fast Fourier transform (FFT), and the energy content is distributed over a small frequency range Δf. In the DPE framework the FFT of the periodic signal is thus used to approximate the single sided PSD by its discrete version $S_k(k \cdot \Delta f)$, feeding it directly to the respective input and propagating the discrete PSD values to the desired performance output. The discrete PSD of the performance output is obtained by summation of the discrete PSD of the propagated periodic signal and discretized versions of the propagated noise PSD models. To estimate the rms value of the performance output y, the integral over the PSD in (1), for calculating the cumulative power spectrum (CPS), is replaced by a discrete summation

$$y_{rms} = \sqrt{CPS_y(f_N)} = \sqrt{\sum_{k=1}^{N} S_{k,y}(k \cdot \Delta f) \cdot \Delta f}. \tag{4}$$

with Δf the frequency sampling rate of the PSD, f_N the Nyquist frequency of the sampled system and $N = f_N/\Delta f$. This enables an integrated DPE framework able to consider stochastic as well as deterministic signals, providing good estimates of several performance outputs of the close-loop controlled mechatronic system, as will be shown in the following. The effects of a potential DC offset on the respective performance output may easily be calculated by the static gain of the system.

3. EXPERIMENTAL SYSTEM DESCRIPTION AND IDENTIFICATION

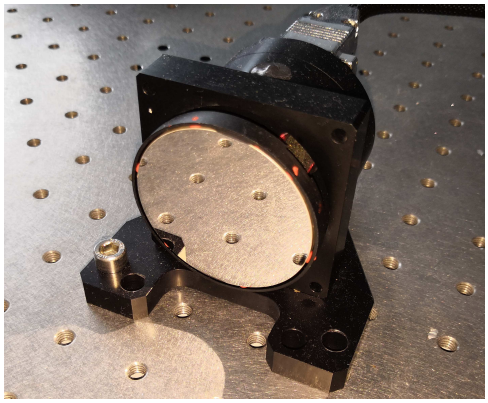

Fig. 1. Commercial fast steering mirror system (OIM102, Optics in Motion LLC, Long Beach, USA). The 2" mirror is actuated by voice coil actuators, while an internal optical sensor measures the mirror position.

To validate the framework for DPE a commercial FSM system (Type: OIM102, Optics in Motion LLC, Long Beach, USA) with a 2 inch mirror and a maximum range of ±26.2 mrad (±1.5 deg) is used (see Fig. 1). The two system axes are actuated by two pairs of voice coil actuators with moving magnets and static coils, operated in push-pull configuration. The position of the flexure guided mover is measured by an internal optical position sensor. In order to have all signals in the system accessible, the commercial drive electronics and control system is replaced. The actuator coils of each axis are directly driven by a custom made voltage controlled current amplifier (OPA544T, Texas Instruments Inc., Dallas, TX, USA). The controller is implemented on a rapid prototyping platform (Type: DS1202, dSPACE GmbH, Germany) running with a sampling frequency of $f_s = 50$ kHz. The rapid prototyping system also implements a rotation matrix to transform the actuator into the sensor coordinate system, which are initially 45° rotated with respect to each other [Csencsics and Schitter (2017b)]. To determine the overall current consumption of the FSM driven in a single (sensor) axis the currents of both actuator axes thus need to be added.

For system identification a system analyzer (3562A, Hewlett-Packard, Palo Alto, CA, USA) is used. The mechanical system with the mirror, the amplifier and the internal sensor are together considered as the plant $G(s)$. The input of the rapid prototyping system, implementing the rotation matrix, is the system input while the position sensor signal is considered as system output. The measured TFs of both mirror axes are identical, as depicted in Fig. 2, and show a suspension mode at about 12 Hz. The cross-coupling between the axes (data not shown) is more than 40 dB lower than the single axis TFs, enabling the use of single-input-single-output controllers. The TF of the

current amplifier (data not shown) with the input voltage of the amplifier as input and the output current considered as the system output shows a flat response with a -3 dB bandwidth of 30 kHz and an amplifier gain of 0.2 V/A. System parameters relevant for the subsequent estimation are summarized in Table 1.

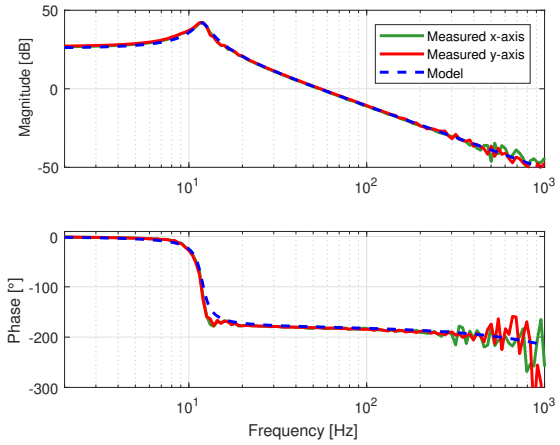

Fig. 2. Frequency responses of the FSM system plant $G(s)$. The response of the FSM x- (solid green) and y-axis (solid red) with suspension modes at 12 Hz are shown together with the system model (dashed blue).

Table 1. System parameters.

Parameter	Value
Sampling frequency f_s	50 kHz
Nyquist frequency f_N	25 kHz
Number of bits	16
Input range	±10 V
LSB voltage q	0.301 mV
Amplifier gain g_a	0.2 A/V
Sensor gain g_s	10/26.2 V/mrad

4. SYSTEM AND SIGNAL MODELING

Before applying the DPE framework the components as well as the noise and signal sources in the system have to be modeled in the frequency domain and according TFs have to be obtained. For this purpose the schematic block diagram in Fig. 3 is considered. It has inputs for the reference signal and the noise sources related to the D/A converter, amplifier, sensor and A/D converter. The performance outputs of interest are the mover position θ_x, the coil current i_{coil} and the tracking error e_x.

4.1 System Modeling

To model the measured frequency response of the plant dynamics (see Fig. 2) a second order model

$$G(s) = K \cdot \frac{\omega_0^2}{s^2 + 2\zeta\omega_0 s + \omega_0^2} \cdot e^{-sT_s} \tag{5}$$

with a DC gain $K = 19.95$ V/V, a suspension mode at 11.9 Hz ($\omega_0 = 74.77$ rad/s), a damping ratio of $\zeta = 0.08$ and $T_s = 20$ μs, representing the sampling delay, is used. The modeled TF is also depicted in Fig. 2.

The dynamics of the amplifier (data not shown) can also be modeled by a highly damped second order system

$$G_A(s) = K_A \cdot \frac{\omega_0^2}{s^2 + 2\zeta\omega_0 s + \omega_0^2} \approx K_A \tag{6}$$

with actuator gain $K_A = 0.2$ A/V, $\omega_0 = 1.885$e5 rad/s and damping ratio $\zeta = 0.8$. As the -3 dB bandwidth of 30 kHz is, however, already larger than the Nyquist frequency of the digital system $f_N = 25$ kHz, the amplifier dynamics in the frequency range of interest can be well approximated by the constant actuator gain K_A.

The optical position sensor system is based on a position sensitive device with analog readout. As there are no additional dynamics obtained in the system identification and spectrum of the sensor noise (see Fig. 4) due to the optical principle and analog readout, the bandwidth of the sensor is considered to be significantly higher than the frequency range of interest, such that it can be modeled by a constant gain

$$G_S(s) = K_{sens} = 0.382 \text{ V/mrad}. \tag{7}$$

The transfer functions of the A/D and D/A converter can be modeled by the dynamics of their anti-aliasing and reconstruction filter, respectively [Riel et al. (2016)]. With cut-off frequencies well beyond 10 kHz, their gains are considered unity for this investigation. To consider the delay of the rapid prototyping system a time delay of half the sampling time is used for each converter, resulting in

$$G_{AD}(s) = G_{DA}(s) = e^{-sT_s/2}. \tag{8}$$

With the dynamics of amplifier, sensor, A/D and D/A converter the dynamics $P(s)$ of the mechanical system with the actuator can be calculated from the measured frequency response $G(s)$ via

$$P(s) = \frac{G(s)}{G_{DA}(s)G_A(s)G_S(s)G_{AD}(s)}. \tag{9}$$

4.2 Position Controller Design and Implementation

As the commercial FSM is a low stiffness system, for which the crossover frequency of the loop gain is typically placed on the mass line [Csencsics and Schitter (2017a)] and as the built-in feedback controller of the commercial FSM is also a PID controller, a PID structure is chosen for designing the feedback controller. The controller is tuned for a loop gain crossover frequency of $f_c = 280$ Hz [Munnig Schmidt et al. (2014)], in order to resemble the closed-loop response with the built-in commercial controller. This results in a second order controller of the form

$$C(s) = K_{PID} \cdot \frac{s^2 + 2\zeta\omega_z + \omega_z^2}{s \cdot (s + \omega_p)} \tag{10}$$

with $K_{PID} = 100.7$, $\omega_p = 6.16$e3 rad/s, $\omega_z = 286$ rad/s and $\zeta = 0.836$. The integrative behavior, which increases the loop gain at low frequencies, is stopped at 45 Hz to enable phase recovery until the crossover frequency at 280 Hz. The differential action generates a phase lead of 55° around the crossover and is stopped by a pole at 980 Hz.

The controller is discretized using Pole-Zero-Matching [Franklin et al. (1997)] for the sampling frequency of

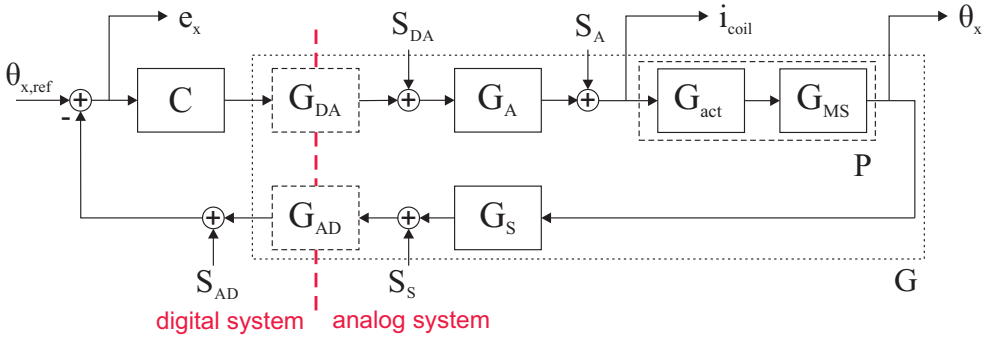

Fig. 3. Block diagram of the position control loop of the FSM x-axis with the individual system components, considered noise and signal sources and the performance outputs coil current i_{coil}, angular position θ_x and error e_x.

f_s = 50 kHz and implemented on the dSpace system. The measured loop gain and complementary sensitivity function (data not shown) show a phase margin of 46° and a -3 dB bandwidth of 550 Hz. As the dynamics of both axes are identical the same controller can be applied.

4.3 Noise and Signal Modeling

The noise characteristics of the individual components in the design phase can typically be modeled based on already existing knowledge or specifications provided in the component data sheets [Fleming (2014)]. For accurate validation of the DPE the noise models of the components are obtained based on previous noise measurements.

A/D Converter. The main noise sources of an ADC can be divided into (i) quantization noise, due to the quantization error made at every sampling step, and (ii) electrical noise of the component [Monkhorst (2004)]. With the 16 bit converters of the rapid prototyping system and an input range of ±10 V the least significant bit (lsb) voltage q = $20/2^{16}$ = 0.305 mV can be obtained. The quantization noise is modeled as white noise with zero mean and a standard deviation of [Oppenheim et al. (1998)]

$$\sigma_{ADq} = \frac{q}{\sqrt{12}} = 0.088 \text{ mV}_{rms}. \tag{11}$$

The electrical noise is obtained with a short circuited input of the ADC and results in a standard deviation σ_{ADe} = 0.29 mV_{rms}, which is significantly larger than the quantization noise. For consideration of low frequency noise components, the ADC noise is modeled by a combination of white and 1/f noise with a corner frequency $f_{nc,AD} = 5$ Hz obtained from the spectrum of the measured electrical noise [Riel et al. (2016)]. The white gaussian noise up to the Nyquist frequency f_N is defined by standard deviations σ_{ADq} and σ_{ADe}, resulting in the PSD model

$$S_{AD}(s) = \frac{\sigma_{ADq}^2 + \sigma_{ADe}^2}{f_N} \cdot \frac{s + 2\pi f_{nc,AD}}{s}. \tag{12}$$

D/A Converter. Since the quantization error introduced by the DAC is similar to that of the ADC and since both have the same lsb voltage value q, the same standard deviation can be used for the quantization noise: $\sigma_{DAq} = \sigma_{ADq} = 0.088$ mV_{rms}. The electrical noise is again obtained by setting the input value of the DAC to zero and measuring the analog output, which results in white noise with a standard deviation of $\sigma_{DAe} = 0.13$ mV_{rms}. The model for the PSD of the DAC up to the Nyquist frequency f_N results to

$$S_{DA}(s) = \frac{\sigma_{DAq}^2 + \sigma_{DAe}^2}{f_N} = 0.9 \cdot 10^{-12} \text{ V}_{rms}^2/\text{Hz}. \tag{13}$$

Amplifier. To get a measure for the noise of the amplifier, the input is short circuited and the output current is measured, resulting in a standard deviation of $\sigma_A = 0.12$ mA_{rms}. The measured signal shows a flat spectrum, such that the PSD model up to f_N can again be calculated by [Jabben (2007)]

$$S_A(s) = \frac{\sigma_A^2}{f_N} = 5.6 \cdot 10^{-13} \text{ A}_{rms}^2/\text{Hz}. \tag{14}$$

Position sensor. For obtaining a model for the position sensor noise, the FSM is situated on a vibration isolation table, the actuator coils are left open and the output signal of the sensor is measured. To also consider the effects of low frequency noise, the sensor noise is modeled by a combination of white and 1/f noise with a corner frequency of $f_{nc,S} = 100$ Hz obtained from the spectrum of the measured noise signal [Riel et al. (2016)]. With the standard deviation of $\sigma_S = 0.73$ mV_{rms} the PSD model up to f_N results to

$$S_S(s) = \frac{\sigma_S^2}{f_N} \cdot \frac{s + 2\pi f_{nc,S}}{s}. \tag{15}$$

The measured and modeled PSD of the sensor noise is illustrated in Fig. 4. The peak value around 10 Hz is explained by the mechanical resonance of the suspended mover, which was not fixed during the measurement, and may be excited by remaining vibrations (e.g. from ground).

Reference signal. As raster trajectories have several frequency components and are commonly used scan trajectories in various optical scanning [Schlarp et al. (2019)] and other imaging applications [Schitter et al. (2008)], a triangular signal with harmonics up to the 11th order

$$\theta_{x,ref} = A\frac{8}{\pi^2}\sum_{k=1}^{11}(-1)^{k-1}\frac{sin(2k-1)2\pi f_r t)}{(2k-1)^2} \tag{16}$$

is used as reference for the fast scanning system axis. The single sided PSD of the reference signal, which is directly

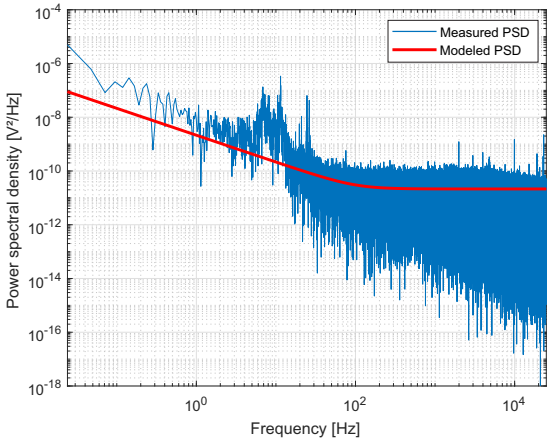

Fig. 4. Measured and modeled PSD of the sensor noise. The white noise level is determined via the measured standard deviation of the time signal.

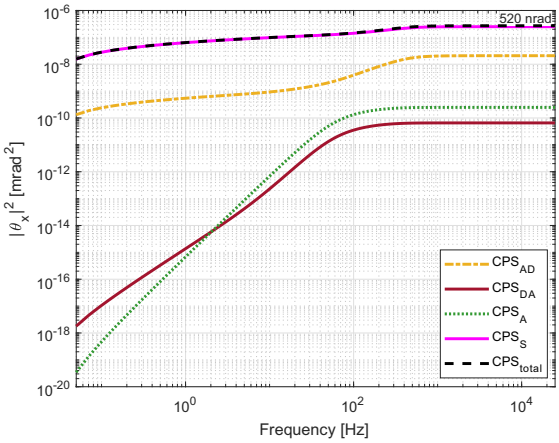

Fig. 5. Simulated cumulative power spectrum (CPS) at the position output θ_x. The contributions of the components and the total resulting CPS is shown.

calculated by using the FFT. For simplicity the reference signal of the slow scanning axis is kept at zero, resulting in a one dimensional scanning motion.

5. EXPERIMENTS AND VALIDATION

The DPE framework is validated by comparing the estimated values for the performance outputs positioning uncertainty, coil current and tracking error, obtained based on the models from the previous section and TFs according to Fig. 3, with measurements of the respective performance output on the commercial FSM system. For evaluation of the estimations for scanning operation, raster trajectories (see (16)) with fundamental frequencies of $f_r = \{10; 30; 50\}$ Hz and various amplitudes A are used as fast axis reference, having their 11th harmonic still covered by the bandwidth of the closed-loop controlled FSM.

For estimating the resulting positioning uncertainty of the closed-loop controlled system, the reference input is set to zero and the PSD models of the contributing noise sources at the position output θ_x are integrated and plotted as cumulative power spectra (CPS) in Fig. 5. The optical position sensor is clearly the dominating disturbance source, followed by the A/D converter. The estimated positioning uncertainty is 0.498 μrad (see (4) and shows reasonable agreement with the measured value of 1.26 μrad, calculated via the rms value of the measured time signal.

To predict combinations of trajectories and scan amplitudes that are feasible to be continuously tracked within the thermal limits of the actuators (and amplifiers), the rms current consumption is evaluated. The rms current limit is set to 800 mA, according to previous experiments. In Fig. 6 the CPS due to the various inputs is depicted at the coil current output for a reference raster trajectory with $f_r = 30$ Hz and $A = 13.1$ mrad. As expected the reference signal $\theta_{x,ref}$ (solid cyan) is the dominating component for the obtained coil current value (dashed black), which results to 570 mA rms. For comparison also the CPS of the measured current (dash-dotted red), which is the sum of the currents through both actuation axes (see

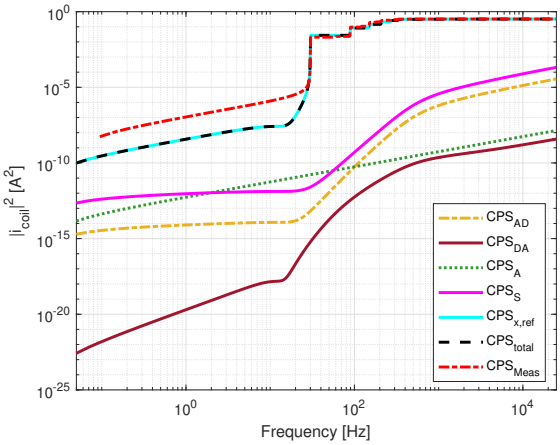

Fig. 6. Simulated cumulative power spectrum (CPS) at the coil current output i_{coil} for a reference raster trajectory with $f_r = 30$ Hz and $A = 13.1$ mrad. The rms current consumption results to 570 mA.

Section 3), is plotted in Fig. 6. It shows good agreement with the estimated CPS, resulting in a current of 550 mA, equaling an estimation error of 3.5%.

In Fig. 7a a comparison of estimated and measured rms coil currents, which are calculated from the measured time signals, is depicted when the FSM is tracking the 10, 30 and 50 Hz raster trajectories with increasing amplitudes. The 50 Hz and 30 Hz trajectory reach the current limit at 7.9 mrad and around 19 mrad, respectively, while with the 10 Hz trajectory scan amplitudes up to the system range are possible. The estimated current values show a linear tendency and represent good estimations for the measured current values of all three trajectories with deviations of 12% rms and 20% max. These deviations may result from unmodeled nonlinearities and crosstalk dynamics.

Considering the rms error for continuous tracking of a scan trajectory, Fig. 7b shows a comparison between the estimated values and measured results, which are again calculated from the measured time signals. The estimated values show again linear relation to the scan amplitude and

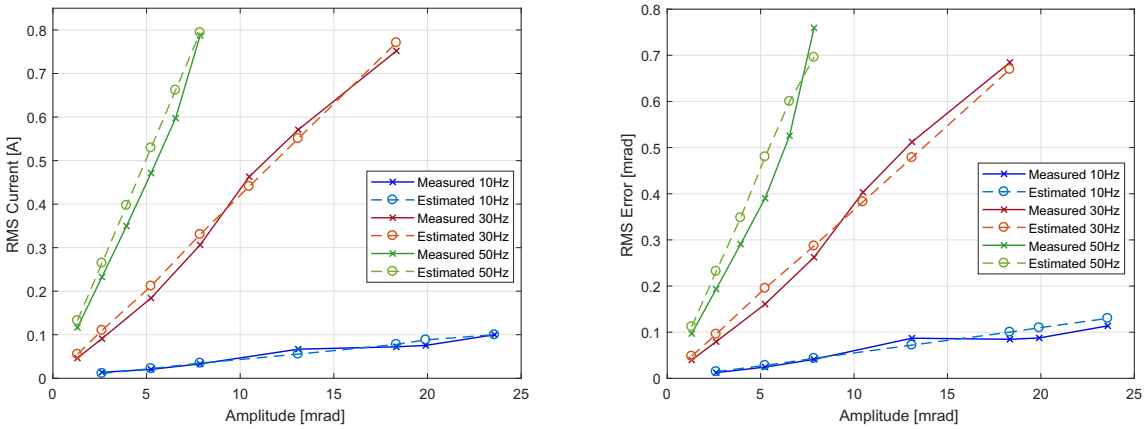

(a) RMS current.

(b) RMS tracking error.

Fig. 7. Comparison of estimated and measured rms values for the performance outputs coil current and tracking error when the FSM is tracking 10 Hz, 30 Hz and 50 Hz raster trajectories of arbitrary amplitude.

are again in good agreement with the experimental results. The relative deviations between estimation and measurement are between 15-17% rms for the tested trajectories.

In summary it is demonstrated that the dynamic performance estimation framework can be used for an efficient prediction of various performance outputs of a mechatronic scanner, including current consumption, tracking error and positioning uncertainty,

6. CONCLUSION

In this paper an integrated framework for dynamic performance estimation of mechatronic scanning systems is presented, capable of properly predicting various performance outputs of the system. The estimation relies on frequency domain models of the individual components and considers stochastic as well as deterministic signals entering the system, providing an integrated design tool. The results of the DPE framework are validated using measurements on a commercial FSM, showing with averaged deviations around 12% for current values and between and 15-17% for tracking error good agreement with the experimental results. Future work is concerned with improving the modeling, including nonlinearities and crosstalk dynamics.

ACKNOWLEDGEMENTS

The financial support by the Christian Doppler Research Association, the Austrian Federal Ministry for Digital and Economic Affairs, and the National Foundation for Research, Technology and Development, as well as MICRO-EPSILON MESSTECHNIK GmbH & Co. KG and ATENSOR GmbH is gratefully acknowledged.

REFERENCES

Avigad, G., Moshaiov, A., and Brauner, N. (2003). Towards a general tool for mechatronic design. *2003 IEEE Conference on Control Applications*, 2, 1035–1040.

Behbahani, S. and de Silva, C.W. (2008). System-based and concurrent design of a smart mechatronic system using the concept of mechatronic design quotient. *IEEE TMECH*, 13(1), 14–21.

Coelingh, E., de Vries, T.J.A., and van Amerongen, J. (1998). Automated performance assessment of mechatronic motion systems during the conceptual design stage. *3rd Int. Conf. on Advanced Mechatronics*, 472.

Csencsics, E. and Schitter, G. (2017a). Parametric pid controller tuning for a fast steering mirror. *1st IEEE CCTA, Hawaii, USA*.

Csencsics, E. and Schitter, G. (2017b). System design and control of a resonant fast steering mirror for lissajous-based scanning. *IEEE TMECH*, 22(5), 1963–1972.

Fleming, A.J. (2014). Measuring and predicting resolution in nanopositioning systems. *Mechatronics*, 24(6), 605.

Franklin, G., Powell, D., and Workman, M. (1997). *Digital Control of Dynamic Systems*. Prentice Hall.

Hedding, L.R. and Lewis, R.A. (1990). Fast steering mirror design and performance for stabilization and single axis scanning. *SPIE Vol. 1304*, 14–24.

Jabben, L. (2007). *Mechatronic design of a magnetically suspended rotating platform*. Ph.D. thesis, TU Delft.

Monkhorst, W. (2004). *Dynamic Error Budgeting: A design approach*. Master's thesis, TU Delft.

Munnig Schmidt, R., Schitter, G., Rankers, A., and van Eijk, J. (2014). *The Design of High Performance Mechatronics*. Delft University Press, 2nd edition.

Okyay, A., Erkorkmaz, K., and Khamesee, M.B. (2018). Mechatronic design, actuator optimization, and control of a long stroke linear nano-positioner. *Precision Engineering*, 52, 308–322.

Oppenheim, A., Schafer, R., and Buck, J. (1998). *Discrete-Time Signal Processing*. Prentice-Hall, Inc., New Jersey.

Riel, T., Saathof, R., Katalenic, A., and Schitter, G. (2016). Noise analysis and improvement of a permanent magnet synchronous motor by dynamic error budgeting. *IFAC-PapersOnLine*, 49(21), 339–346.

Saathof, R., Thier, M., Hainisch, R., and Schitter, G. (2017). Integrated system and control design of a one dof nano-metrology platform. *Mechatronics*, 47, 88–96.

Schitter, G., Thurner, P., and Hansma, P. (2008). Design and input-shaping control of a novel scanner for high-speed afm. *Mechatronics*, 18(5), 282.

Schlarp, J., Csencsics, E., and Schitter, G. (2019). Optical scanning of a laser triangulation sensor for 3d imaging. *IEEE TIM*, in print.